Polymer Testing 109 (2022) 107530

Contents lists available at ScienceDirect

Polymer Testing

journal homepage: www.elsevier.com/locate/polytest

# Sustainable terpene triblock copolymers with tuneable properties for pressure sensitive adhesive applications☆

M.T. Elsmore [a], R.L. Atkinson [b], D.J. Irvine [a], S.M. Howdle [b], D.S.A. De Focatiis [a,*]

[a] Faculty of Engineering, University of Nottingham, Nottingham, NG7 2RD, UK
[b] School of Chemistry, University of Nottingham, Nottingham, NG7 2RD, UK

ARTICLE INFO

*Keywords:*
Terpenes
Renewable
Elastomer
Pressure sensitive adhesive
Triblock copolymer

ABSTRACT

A series of triblock copolymers in a hard-soft-hard block configuration with varying hard block α-pinene methacrylate content and molecular weight and butyl acrylate soft segment have been synthesised and investigated for viability in pressure sensitive adhesive (PSA) applications. The morphologies vary from pockets of hard phase distributed within a continuous soft matrix, through to lamellar with co-continuous phases, and finally continuous hard phase with pockets of soft phase dispersed. Uniaxial tensile properties, probe adhesion performance and cyclic adhesive behaviour are presented for seven compositions including four short chain and three long chain copolymers, alongside a commercial benchmark PSA. Structure-property relationships for the novel elastomers are evaluated, establishing that short chain materials with 20–25 wt% poly(α-pinene methacrylate) offer similar tensile and adhesion performance to the commercial elastomer. Raising the hard phase concentration has been observed to provide a considerable increase in ultimate tensile strength, stiffness and peak tack force, but at the expense of significant reductions in ultimate tensile strain, adhesive bond displacement and vibrational dissipation. The results suggest that the performance of these sustainable materials can be tuned to produce viable PSAs with a range of useful properties.

## 1. Introduction

Pressure sensitive adhesives (PSAs) find application across a wide range of industries, including medical adhesives [1], drug delivery [2], textiles [3], automotive [4] and general household DIY [5]. PSAs are viscoelastic in nature and maintain their physical state, as opposed to common adhesives such as glues and resins which instead solidify or cure, resulting in permanent adhesion to the substrate materials [6]. The ability of pressure sensitive materials to be removed following adhesion and in some cases to be re-used provides a useful facility for temporary fixings, or where non-permanent adhesion is desirable, such as to enable components to be more easily recycled. Their ability to adhere to a variety of substrates, to form a strong adhesive bond, and their ease of application make PSAs an effective alternative to mechanical or chemical fastening. The adhesion process for these materials is far quicker than for most curing or solvent-loss systems, with bonding typically occurring over timescales of <60 s [7].

The main characteristics of PSA materials are low stiffness, tacky behaviour and an ability to adhere when subjected to low contact pressures [8]. PSAs typically consist of low glass transition ($T_g$) cross-linked elastomers [9] or block copolymers containing a low glass transition elastomeric soft phase between high glass transition blocks which act as physical crosslinks [10]. An advantage of thermoplastic elastomers is their melt processability, owing to the thermoplastic nature of both the hard and soft blocks, allowing for extrusion or moulding of complex shapes as well as recyclability [11].

The majority of pressure sensitive materials are synthesised from natural or synthetic rubber, including poly(acrylates), silicones, polyvinyl ethers and urethanes [12,13]. Most PSA materials on the market today are manufactured from monomers derived from crude oil. Based on a study conducted in 2015 by the International Food and Agribusiness Management Association (IFAMA), polymer production comprises 7% of all crude oil use [14], with over 300 million tonnes of synthetic polymer materials being produced each year [15]. The terpene family of organic compounds is a source of monomers that has been the focus of many recent scientific investigations owing to their potential for use as high $T_g$, glassy homopolymers [16] and adhesive resins [17]. A popular renewable source of monoterpenes is turpentine from pine wood, which

☆ *use adhesive and copolymer in place of last 2 if phrases not allowed.

* Corresponding author.
*E-mail address:* davide.defocatiis@nottingham.ac.uk (D.S.A. De Focatiis).

https://doi.org/10.1016/j.polymertesting.2022.107530
Received 21 September 2021; Received in revised form 14 February 2022; Accepted 2 March 2022
Available online 10 March 2022

is processed to produce α and β-pinene for further functionalisation and subsequent polymerisation [18,19]. According to a 2010 study conducted by the governmental Department for Environment, Food and Rural Affairs (DEFRA), the UK alone produces 4.3 million tonnes of waste wood material each year, which offers a sizeable waste feedstock for novel polymer production [20]. Replacement of an oil-based polymer with a sustainable material developed from pinene monomers would help to significantly reduce consumption of finite fossil fuels and may offer a cheaper and more environmentally friendly alternative to current commercial materials.

The use of biomass derivatives in pressure sensitive compounds is not uncommon. Wang and co-workers found that use of 4-propylsyringyl acrylate derived from lignocellulosic biomass as a hard phase material in a triblock copolymer with *n*-butyl acrylate functions as an effective pressure sensitive adhesive [21]. They observed that the adhesive strength and failure properties of the lignin-based copolymer rival those of Fisherbrand and Scotch tapes, and hence could be used as a sustainable alternative. Lee et al. examined the pressure sensitive behaviour of renewable thermoplastic elastomers synthesised from fatty acids, corn starch, rosin and soybean oil [22]. They found that increasing the hard phase weight fraction resulted in an increase in tensile failure stress and stiffness as well as in the elastic storage modulus. A rise in adhesive tack force, 180° peel strength and shear strength with increasing hard phase concentration was also observed, with stress magnitudes similar to those exhibited by commercial materials.

Tackifying behaviour is a notable characteristic of terpenoid materials making them suited to use in adhesives, and commonly found in masking tapes, laminating and rubber solution adhesives and hot melt coatings [23]. A recent study conducted by Droesbeke et al. showed potential for PSA materials produced from various cross-linked terpenoid latexes, including tetrahydrogeranyl acrylate, menthyl methacrylate, citronellyl methacrylate and isobornyl methacrylate. Measurements of dynamic shear modulus indicated general purpose and high shear pressure sensitive adhesion applications, with accompanying probe tack, loop tack, peel and shear adhesion measurements confirming promising PSA properties, with peak probe adhesive stresses ranging between 200 and 600 kPa, depending on composition [24].

This study looks at the use of α-pinene methacrylate [18] as the polymeric hard phase component in a series of triblock copolymers with butyl acrylate of varying composition. The effects of poly(α-pinene methacrylate) concentration and overall chain length on mechanical and adhesion performance are investigated to identify suitability of these materials as renewable pressure sensitive adhesives and to better understand the influence of copolymer composition on physical properties relevant to adhesive applications.

## 2. Materials

### 2.1. Synthesis

For both monomers, α-pinene methacrylate (obtained from Cornelius Specialities) and butyl acrylate (99% BASF), the inhibitor was removed via an alumina column prior to use. The reversible addition-fragmentation chain transfer (RAFT) agent, S,S′-bis(α,α′-dimethyl-α′’-acetic acid)-trithiocarbonate (BDAT), was synthesised following a standard method [25]. 2,2-Azobis(2-methylpropionitrile) (AIBN, 98% Sigma Aldrich) was re-crystallised twice before use. All other reagents were purchased from Sigma-Aldrich and used as purchased.

The RAFT agent, BDAT (varying mol%) was added as a solid to the reaction vessel, and the monomer (5 g) and AIBN (0.2 mol% of BDAT) were then completely dissolved in toluene (5 mL) and added to the reaction vessel. The system was degassed using three freeze-pump-thaw cycles to ensure an oxygen free environment, then placed under argon and heated to 75 °C. The polymerisations were terminated below 60% conversion to retain chain end fidelity. The reactions were monitored using $^{1}$H NMR and, when nearing 60% conversion, the reaction mixture was exposed to air to quench the radicals. The resulting poly(α-pinene methacrylate) (αPMA) macro-RAFT agent was purified by dissolving the reaction mixture in a minimum of tetrahydrofuran (THF) and precipitating into ice cold methanol, then filtered using Buchner filtration. This precipitation step was carried out 2–3 times until all monomer was removed, and then the polymer was dried under vacuum at 25 °C.

To synthesise the ABA triblock copolymer, the chosen αPMA macro-RAFT agent (2 g) was combined with butyl acrylate, varying the quantity depending on the desired wt%, and with AIBN (0.2 mol% wrt macro-RAFT agent) and toluene (1:1 w/v ratio of total monomer to solvent) to form a poly(butyl acrylate) (BA) block. The reaction was carried out and analysed using the same methods and techniques as for the homopolymerisations and was allowed to reach full conversion at 65 °C. Further details on the synthesis of the novel elastomers investigated within this work can be found in [26].

### 2.2. Polymers

Triblock copolymers of poly(α-pinene methacrylate)–B–poly(butyl acrylate)–B–poly(α-pinene methacrylate) in a hard-soft-hard block configuration have been synthesised via RAFT polymerisation to give a range of hard phase volume fraction variations. Table 1 reports gel permeation chromatography (GPC) measurements of the number average molecular weights, $M_n$, of the block copolymers assessed within this study. In addition to varying the proportion of hard to soft phase material, the copolymer chain molecular weight was also varied, and the materials have been categorised into two families: short (<12 kDA) and long (>12 kDa) end blocks. Molecular weight distributions are given in Figs. S1(a) and (b).

A commercially available PSA material developed by Velcro Industries B.V. and commercialised under the trade name ‘FIX-PRO® mounting tape’ was purchased from Screwfix Direct Ltd and employed as a benchmark product for establishing application suitability. Election of this material as a benchmark comparison was based upon similarity in the available thickness and general behaviour during manual handling, with the aim of identifying the novel elastomers’ viability for the intended application. The product was acquired in 1 mm thick sheet form, packaged as a roll 25 mm in width, with a soft, removable polymeric backing tape. FIX-PRO® is marketed as a removable adhesive material for use in home DIY repair applications, for wall mounting of items such as clothing hooks, picture frames and as a general alternative to mechanical fasteners in low load-demanding applications [27].

### 2.3. Specimen preparation

Films of nominal thickness ~0.5 mm were produced via solution casting in THFsolvent, using 10 wt% copolymer to 90 wt% solvent proportions, onto an ethylene tetrafluoroethylene (ETFE) film. The same solvent was used for casting all samples to ensure no variability due to solution dispersion [28].

Samples were dried under a fume hood overnight to evaporate the majority of the solvent, and then transferred to an unheated vacuum

**Table 1**
Molecular weight configurations for short and long chain α-pinene derived copolymer materials.

| Chain length | Material | $M_n$ configuration (kDa) | [αPMA] (wt %) | Total chain $M_n$ (kDa) |
|---|---|---|---|---|
| **Short** | αBα-74-23 | 8.5–56.8 – 8.5 | 23 | 73.8 |
| | αBα-70-24 | 8.4–53.1 – 8.4 | 24 | 69.8 |
| | αBα-64-28 | 9.0–46.4 – 9.0 | 28 | 64.4 |
| | αBα-60-33 | 9.9–40.3 – 9.9 | 33 | 60.2 |
| **Long** | αBα-114-24 | 13.7–86.6 – 13.7 | 24 | 114.0 |
| | αBα-91-30 | 13.6–63.5 – 13.6 | 30 | 90.7 |
| | αBα-91-42 | 19.2–53.0 – 19.2 | 42 | 91.4 |

oven for 5 days to ensure complete solvent removal. This was confirmed by thermogravimetric analysis (TGA) as no mass loss could be detected around the solvent's boiling point. Following vacuum drying, the elastomer film was carefully peeled off the ETFE substrate and cut into rectangular strips for tensile testing using a pair of fixed separation razor blades, or into an 8 mm disc using a sharp steel punch for probe adhesion or rheological testing. Whilst thermoplastic elastomers can be moulded using thermal processes, solution casting is more suited to the smaller quantities of material available. It also reduces likelihood of void formation due to bubbles, leads to a greater degree of phase separation and can provide a relatively uniform film thickness.

Rectangular bar specimens of FIX-PRO® for use in tensile experiments were cut from the roll material following the same method as for the solution cast triblock samples and the backing tape was removed prior to testing. 8 mm discs were also punched directly from the roll for use in adhesion and rheological experimentation with the backing tape removed.

## 3. Methodology

*Gel permeation chromatography* (GPC) was used to acquire molecular weight and dispersity data for the polymers. An Agilent 1260 infinity multidetector SEC system, with a multi angle light scattering detector (MALS, Wyatt, Optilab Dawn 8+), was coupled to a Viscometer (Wyatt, ViscoStar-2) and a differential refractometer (DRI, Agilent 1260) for sample detection. The columns used were 2 x Agilent PLGEL 5 μm Mixed D (7.5 mm × 300 mm) and a PLGEL 5 μm guard column (7.5 mm × 50 mm). The mobile phase was THF at 1 mL $min^{-1}$ at 40 °C. A known refractive index increment ($dn/dc$) value of 0.067 mL $g^{-1}$ was used for poly(butyl acrylate) [29]. *A* $dn/dc$ value of 0.106 g $mol^{-1}$ was measured for Poly(α-pinene methacrylate) using light scattering calibration. For the block copolymers, $dn/dc$ was determined using [30]

$$\frac{dn}{dc_{(P1-b-P2)}} = m_{(P1)}\frac{dn}{dc_{(P1)}} + m_{(P2)}\frac{dn}{dc_{(P2)}} \tag{1}$$

where $m_{(P1)}$ and $m_{(P2)}$ are the mass fractions of the individual block components.

Poly(α-pinene methacrylate) homopolymers were measured by comparison with poly(methyl methacrylate) (PMMA) standards (12 PMMA standards across a range of $M_n$ from 1 to 400 kDa), as the values obtained from light scattering were found to be inconsistent.

*Atomic force microscopy* (AFM) images were obtained on spin-cast samples using a Dimension FastScan AFM (Bruker Corporation), working in PeakForce quantitative nanomechanical property (PF-QNM) mode in air with an RTESPA-150 silicon probe (spring constant = 2.44 N $m^{-1}$). Specimens were prepared by dissolving 30 mg of polymer in 1 mL of toluene, then spin coating the solution onto a silicon wafer at 1500 rpm for 30 s. The resulting thin films were annealed at 180 °C for 24 h, after which the oven was turned off and allowed to cool slowly to room temperature.

*Dynamic mechanical analysis* (DMA) was performed using a Triton Technology DMA (TTDMA) using a powder pocket accessory. Approximately 40 mg of material was added to the powder pocket. Measurements were conducted at a frequency of 1 Hz in single cantilever bending mode whilst increasing temperature $T$ at a rate of 10 °C per minute from −60 to 200 °C. $T_g$ values were obtained from the peaks in the loss tangent.

*Stress-strain measurements* were performed using one of three techniques, depending on the stiffness of the material: twin drum Sentmanat extensional rheometry (SER), miniature uniaxial tensile testing using a Linkam fixture, or miniature flexural 3-point bending using an in-house fixture. The physical behaviour of the elastomers varied significantly, from soft and stretchy to hard and brittle, thus requiring different instrumentation to obtain the mechanical response. All testing was conducted at standard laboratory conditions of (22.0 ± 0.3) °C.

Rectangular bar specimens used in SER and Linkam tensile experimentation were scanned at high resolution to obtain the width. ImageJ software was employed to accurately measure the width at 5 points along the profile of each specimen. Thickness measurements were obtained using a Hildebrand thickness gauge with a probe of diameter 4 mm and mass of 27.6 g following 2 minutes of compression. As many of the specimens were highly compressible, the direct measurement does not represent the true, uncompressed specimen thickness, and an iterative correction was applied based on Lebedev [31]. This technique uses values of stiffness established from the mechanical tests and assumes isochoric deformation, which is typical for elastomers of this type [32]. For each iteration, a correction to the measured thickness is applied until a steady state value is obtained. This is then considered an accurate representation of the true specimen thickness under the absence of load.

A twin drum SER system was employed on an Anton Paar MCR302 rheometer for soft samples that deformed to large strains, and where sufficient flexibility enabled specimens to be wrapped around the drums. As illustrated in Fig. 1(a), rectangular strips of dimensions ca. 0.5 x 5 × 25 $mm^3$ were subjected to a constant true strain rate elongation of 3% $s^{-1}$ until specimen failure. Nominal (engineering) stress $\sigma$ and strain $\varepsilon$ were determined from device measurements of torque $M$ and shaft rotation rate Ω as functions of experiment time $t$, and are given by [33]

$$\sigma(t) = \frac{M}{2(1+\varepsilon)Rd_0w_0\exp(-\dot{\varepsilon}t)} \tag{2}$$

and

$$\varepsilon(t) = \exp\left(\frac{2\Omega Rt}{L_0}\right) - 1 \tag{3}$$

where $R$ is the drum radius, $L_0$ is the distance between drum centres, $d_0$ is the initial specimen thickness, $w_0$ is the initial specimen width, and $\dot{\varepsilon}$ is the applied true strain rate. This technique was similarly employed in a prior study assessing the tensile properties of soft silicones which exhibited low tear strengths and stiffnesses ranging ~50–180 kPa, making them unsuitable for clamping using conventional methods [34].

For specimens that were too stiff to be wrapped around the SER drums yet still sufficiently elastic in nature, a Linkam TST350 miniature tensile testing stage fitted with a 20 N load cell, illustrated in Fig. 1(b), was employed. Specimens were cut to the same dimensions as used in SER experimentation and subjected to a constant nominal strain rate of 3% $s^{-1}$ until failure. To prevent contact between the specimen and the heater giving rise to frictional forces, 1 mm thick spacers were laser cut from PMMA sheet and added to each grip, raising the specimen above the heater. For all miniature tensile tests, a starting gauge length of 15.2 mm was applied.

Miniature flexural 3-point bending was performed using an in-house fixture illustrated in Fig. 1(c) and described in detail in [35], for stiffer elastomers which exhibited brittle behaviour and could not be accurately measured using tensile methods due to gripping difficulties. Rectangular bar specimens of dimensions 0.5 x 2 × 7 $mm^3$ were cut from a solution cast sheet using parallel razor blades and measurements of thickness and width obtained following the same methods as for rectangular bars used in SER and miniature tensile experimentation. The miniature specimens were subjected to 3-point bending with a span distance of 5.535 mm between supports using a loading probe with 0.5 mm nose radius at a constant nominal strain rate of 0.05% $s^{-1}$ until specimen failure. A 10 N load cell was used to obtain measurements of force.

*Cyclic uniaxial tensile testing* was conducted using a solid rectangular fixture (SRF) attached to an Anton Paar MCR302 rheometer, as illustrated in Fig. 1(d). Masking tape was applied to the grips of the SRF and specimens of dimensions 0.5 x 5 x 25 $mm^{-3}$ adhered to the tape using a cyanoacrylate adhesive and hand tightened to prevent slip during tensile deformation. Specimens were subjected to cyclic loading and unloading at constant nominal strain rates of 3% $s^{-1}$. During the unloading stages,

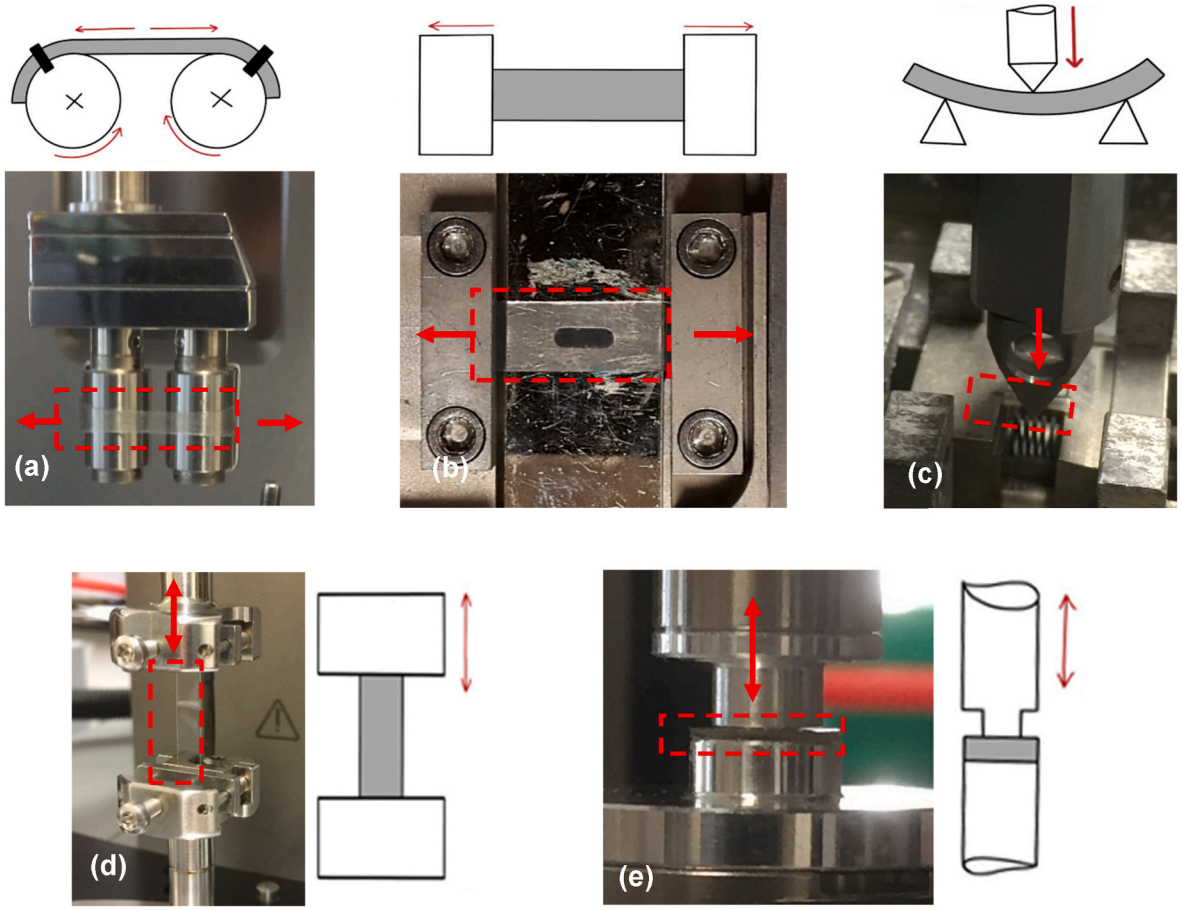


**Fig. 1.** Photographs and schematics of experimental conditions for (a) SER tensile testing, (b) miniature tensile testing, (c) miniature flexural 3-point bending, (d) SRF cyclic tensile testing and (e) probe adhesion, all conducted on transparent elastomers which are difficult to see. Red dashed boxes indicate specimen locations and arrows show the directions of displacements. In the accompanying schematics the grey profile represents the specimen.

a minimum tensile normal force of 0.1 N was maintained to prevent the specimens from buckling.

*Probe adhesion testing* was conducted using an Anton Paar MCR302 rheometer customised with an upper contact probe consisting of a flat plate machined to a diameter of 5.8 mm and a surface roughness of $R_a$ = 0.8 μm for the purpose of butt adhesion tests, and a lower 8 mm plate, as illustrated in Fig. 1(e). ~0.5 mm thick discs 8 mm in diameter were carefully placed on the lower plate and light pressure was applied to adhere the specimen to the plate. During the measurement the upper probe was brought into contact with the test specimen at a constant speed of 10 μm $s^{-1}$ until a force of −10 N (region A in Fig. 2), held at constant position for 60 s (region B), and retracted at a constant speed of 1.25 μm $s^{-1}$, as illustrated in Fig. 2. While the upper plate was retracted, the normal force was recorded as a function of gap height $d$, first rising towards a maximum (region C) and then reducing until loss of contact (region D). The starting thickness $d_0$ is identified as the gap height at $F$ = 0 N, and the peak adhesive force $F_{max}$ as the normal force maximum. Adhesion results presented throughout this study correspond to measurements of displacement beyond $d_0$. Experimental timescales of detachment ranged from little over 1 minute, for stiffer materials, to as much as 11 minutes, for softer materials, from initial probe contact to complete detachment.

The chosen application force of 10 N corresponds to a compressive stress of 378 kPa on the specimen. Based on a crude estimate of thumb contact area of 400 $mm^2$ and anthropometric data for maximum thumb force exertion ranging ~170–250 N [36], equating to stresses of 425–625 kPa, the chosen loading conditions are of comparable magnitude to moderate manual pressure.

## 4. Results

### 4.1. Triblock copolymer structure and morphology

The morphology arising from phase separation of the hard and soft blocks can strongly influence the mechanical performance of a block copolymer [37,38]. Morphological structures acquired using AFM are shown in Fig. 3.

As the concentration of hard phase is increased, there is a clear evolution from small spherical hard phase regions distributed within a continuous soft BA matrix ([αPMA] < ~0.25) to a lamellar morphology with both phases co-continuous (~0.25 < [αPMA] < ~0.4), to a structure with spherical soft phase regions distributed within a continuous hard phase ([αPMA] > ~0.4), and this is consistent for both long and short chain materials. Examining copolymers with a similar hard phase concentration but different overall (and individual component) chain lengths (eg. comparing αBα-74-23 and αBα-70-24 to αBα-114-24, and comparing αBα-64-28 and αBα-60-33 to αBα-91-30), we can observe qualitatively that the characteristic length scale of the regions increases with increasing molecular weight, and hence with chain length.

The loss tangent from a DMA measurement performed on a specimen of αBα-91-42 is shown in Fig. 4 and indicates the presence of two distinct $T_g$s attributable to the hard and soft phase at −28 and 167 °C respectively. The large window between the BA and αPMA block $T_g$s indicates a broad service temperature range for this family of novel triblock materials. It was not possible to determine $T_g$s in the other materials using the same method due to the challenging nature of the powder pocket set-up, but they are expected to be approximately similar.

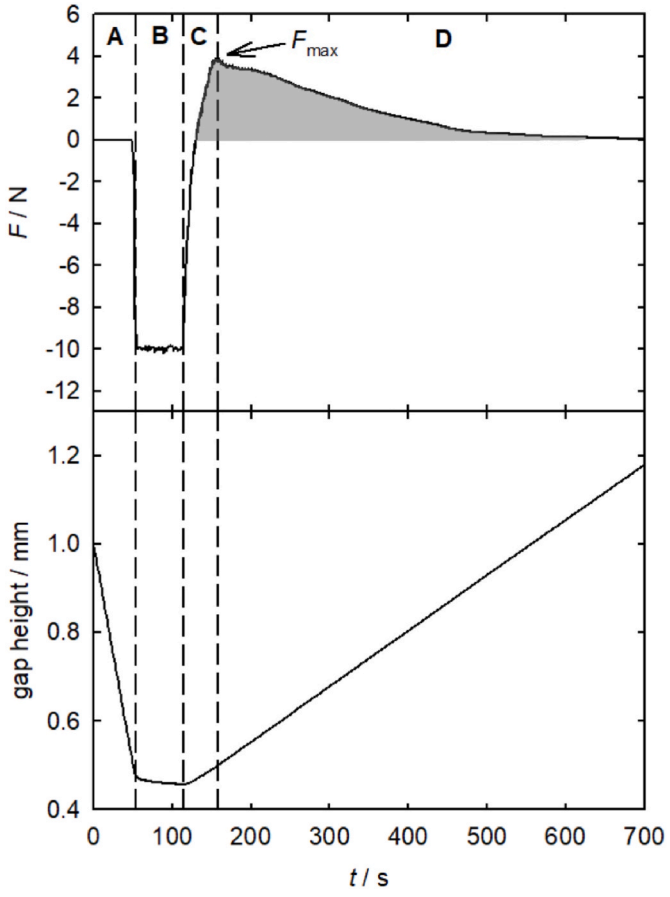


**Fig. 2.** Method for analysis of probe tack adhesion data showing compression (A), dwell period (B) and retraction (C & D) stages of the experiment. Positive force measurements indicate adhesion and negative measurements indicate a compressive force.

### 4.2. Mechanical performance of α-PMA triblock copolymers

Uniaxial tensile testing or 3-point bending was conducted to establish the mechanical response of the pinene-derived copolymers. Fig. 5 shows measurements of the average stress vs strain of the short and long chain copolymers, until the strain value of the specimen which failed first. The SER drums were used for measurement of 23, 24 and 28 wt% short chain copolymers and for the 24 and 30 wt% long chain copolymers. For the 33 wt% short chain material, which exhibited much stiffer behaviour and was incapable of being wrapped around the SER drum fixture, the Linkam miniature tensile device was used. The 42 wt% long chain specimens were brittle and too challenging to clamp with mechanical grips and had to be tested in flexural mode in 3-point bending. Whilst the bending data is mixed-mode tension and compression, and at a reduced strain rate, and hence not directly comparable with the tensile data, it does provide an indication of relative mechanical performance, at least at low strains. Table 2 shows a summary of mechanical properties for the copolymers and the number of specimens examined in each case. Specimen availability was limited due to the pre-scale up nature of these novel copolymers as well as the quality and uniformity of the cast films, but a minimum of 4 specimens were tested for each sample and more where available.

It is evident from the data that, irrespective of soft segment molecular weight, increasing [αPMA] results in an increase in the tensile stress at a given applied strain. The ultimate tensile stress $\sigma_{UTS}$ and ultimate tensile strain $\varepsilon_{UTS}$ were established at the point of maximum stress and are provided along with values of secant modulus at 1% strain $E_{1\%}$ and 10% strain $E_{10\%}$ in Table 2. It was not possible to determine $E_{10\%}$ for αBα-91-42, as brittle failure occurred at ~4% flexural strain.

It is worth noting that in the αBα-60-33 material, the peak stress occurs at ~57% strain, but the material continues to flow at approximately constant stress and only fails at ~200–250%. This is likely to be attributed to plasticity in the continuous hard phase. This behaviour was found to be repeatable for all 4 specimens tested and similar behaviour has been observed in a previous study on filled polyacrylate systems [39]. All other materials investigated failed shortly after reaching $\varepsilon_{UTS}$.

Four cycles of tensile loading and unloading through to 25% strain and down to 0.1 N were performed on single specimens of αBα-70-24 and on the benchmark FIX-PRO® elastomer, producing the results shown in Fig. 6. These measurements provide an indication of material performance during re-use, replicating the mode of deformation as a result of manual stretching or during repeated application and peeling from a substrate. Following a single 25% load-unload cycle, αBα-70-24 and FIX-PRO® were found to exhibit residual strains (at an unloading force of 0.1 N) of 19.4% and 12.3% respectively, increasing to 21.9% and 13.2% after a further three load-unload cycles. With successive deformations, the maximum stress achieved at 25% strain is shown to reduce by 28.6% for αBα-70-24 and by 6.7% for FIX-PRO® between the first and fourth cycles. The increase in residual strain over the four cycles is similar for the two materials, despite a factor of 1.6 difference in the measured residual strain magnitudes and noticeably different cyclic stress profiles. The cyclic tests show that a large degree of plastic deformation has taken place in the αBα-70-24, unlike the commercial material which performs in a more elastic manner.

Fig. 7 provides cyclic data up to $\varepsilon = 100\%$ for the two elastomers, following the pseudo-cyclic strain history shown in the inset. Results obtained for the αPMA triblock copolymer suggest more significant energy dissipation between loading and unloading cycles. Conversely, FIX-PRO® shows a lower energy dissipation as a result of cycling to increasing strains. The pseudo-cyclic performance exhibited by the novel terpene-based elastomer is similar to that of some thermoplastic polyurethane (TPU) block copolymers [40]. Based on these findings, it is possible that the novel material may be better suited to applications where a greater degree of damping is beneficial, such as where the ability to dissipate sound or vibration is favourable.

Due to limitations in material availability, it was only possible to perform cyclic testing on the αBα-70-24 terpenoid elastomer. Hence, the influence of chain length and phase concentration on the cyclic properties has not been confirmed. Scmaltz and co-workers conducted pseudo-cyclic tensile experiments on polystyrene-*block*-poly-(ethylene-*alt*-propylene)-*block*-polyethylene (PS-B-PEP-B-PE) triblock copolymers with crystalline PE hard phase concentrations of 22 and 30 wt%. 3 hysteresis cycles to $\varepsilon = 100\%$ were performed on both samples showing small increases (~0.5–1%) in residual strain for each successive cycle for both materials, with the 30 wt% variant exhibiting greater plastic deformation. Further successive hysteresis cycles to $\varepsilon = 500\%$ in 100% intervals were performed, giving increasing residual strains per cycle for both copolymers, with residual strains of 60.6% and 76.2% for the 22 and 30 wt% variants respectively [41].

It is postulated therefore that high [αPMA] elastomers are likely to deform in a predominantly plastic manner, with larger residual strains and higher energy losses caused by the plastic strain within the hard domains. Conversely, low [αPMA] copolymers are expected to exhibit much smaller residual strains due to the more elastic behaviour imparted by the dominant soft phase, and lower hysteretic energy losses due to the rubbery nature of the BA.

### 4.3. Probe adhesion performance of PSAs from α-pinene

For an elastomer to function as a PSA, it must be capable of providing a sufficient degree of adhesive strength. The ability form a strong adhesive bond is known to be a function of a number of factors including, but not limited to, substrate material [42], surface roughness [43] and application temperature and humidity [44]. Elastomer disc specimens of

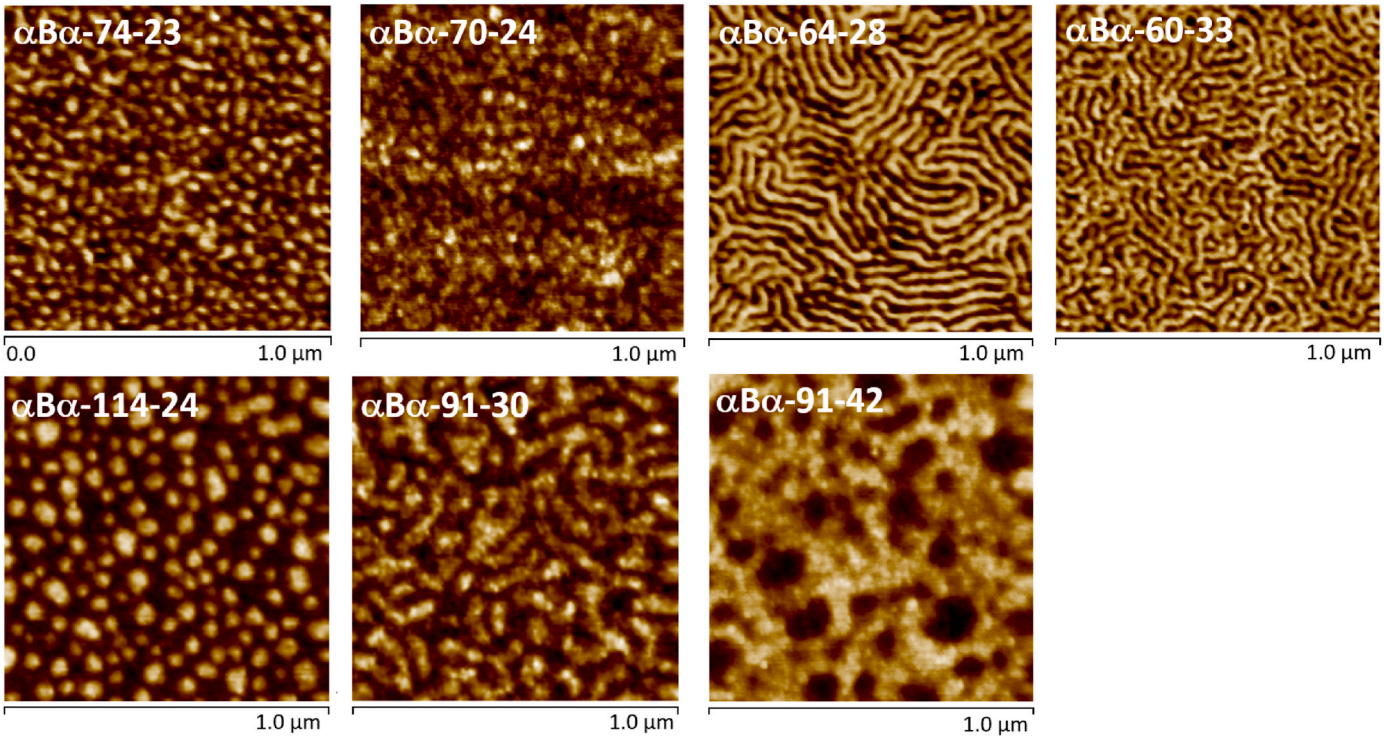


**Fig. 3.** AFM images of a 1 $\mu m^{-2}$ area for novel αPMA triblock copolymers. Short chain materials are given in the top row and long chain materials in the bottom row. Light and dark regions correspond to the αPMA (hard phase) and BA (soft phase) fractions respectively.

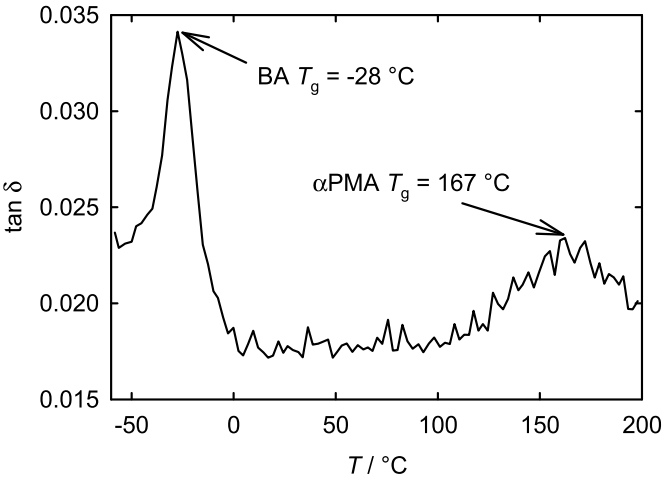


**Fig. 4.** Powder pocket cantilever powder-pocket flexural measurements of loss tangent conducted on αBα-91-42, showing peaks at −28 and 167 °C, corresponding to BA and αPMA block $T_g$s respectively.

8 mm diameter were subjected to probe adhesion experimentation using a 5.8 mm aluminium probe under consistent laboratory environmental conditions of temperature and humidity. The same aluminium probe with a reproducible surface roughness of $R_a = 0.8$ μm was used for all experiments and was cleaned with a suitable solvent before and after tests to remove residual material. Fig. 8 shows values of adhesive force $F$ as a function of normalised displacement up to a peak force $F_{max}$ for 3 specimens of each of the short and long chain αPMA triblock copolymers, and on 5 specimens of FIX-PRO®, illustrating the performance of the unbroken adhesive bond. The magnitude of [αPMA] has a small effect on adhesive bond strength, increasing with increasing [αPMA]. Probe displacements $d$ have been normalised by $d_0$ to account for differences in cast film thickness.

To assess the work done per unit volume $W$ in full detachment, a single specimen of each material was subjected to a full detachment cycle, providing the representative results shown in Fig. 9. $W$ was calculated as the area under the normalised force-displacement curves based on an effective volume of material under the probe. This assumption undoubtedly produces a slight overestimate in the magnitude of $W$, as the material deforming under the probe is a little larger than the circumference of the probe, and as such should be considered an upper bound.

The 23 and 24 wt% short chain and 24 wt% long chain terpenoid elastomers exhibit similar curve shapes to the commercial material. These results indicate that for the adhesion conditions examined, copolymers with [αPMA] = 20–25 wt% will provide similar performance to the elected benchmark. Average results from adhesion testing of the long and short chain terpene-based copolymers along with FIX-PRO® are provided in Table 3.

During use, a PSA material has the potential of being removed and re-applied to a surface multiple times. To determine how the novel materials would perform under such conditions, the elastomers were subjected to 5 additional bond-debond cycles following the initial cycle. As shown in Fig. 10, αPMA elastomers exhibited an average drop in $F_{max}$ of 22% between the 1st and 2nd cycles, with the exception of αBα-91-30, compared to 5.9% as measured for FIX-PRO®. αBα-74-33 provides the smallest loss of adhesive strength with repeated application, followed closely by the lowest [αPMA] short and long chain variants. Thus, following destruction of the first surface bond, adhesive performance remains relatively consistent during a moderate number of further usage cycles for both the αPMA and commercial materials, decreasing by a small amount with each successive cycle. For αBα-91-30 however, the opposite behaviour is observed, with $F_{max}$ increasing on average by 11.6% over the 6 cycles.

## 5. Discussion

In a standard application, a typical PSA elastomer is subjected to

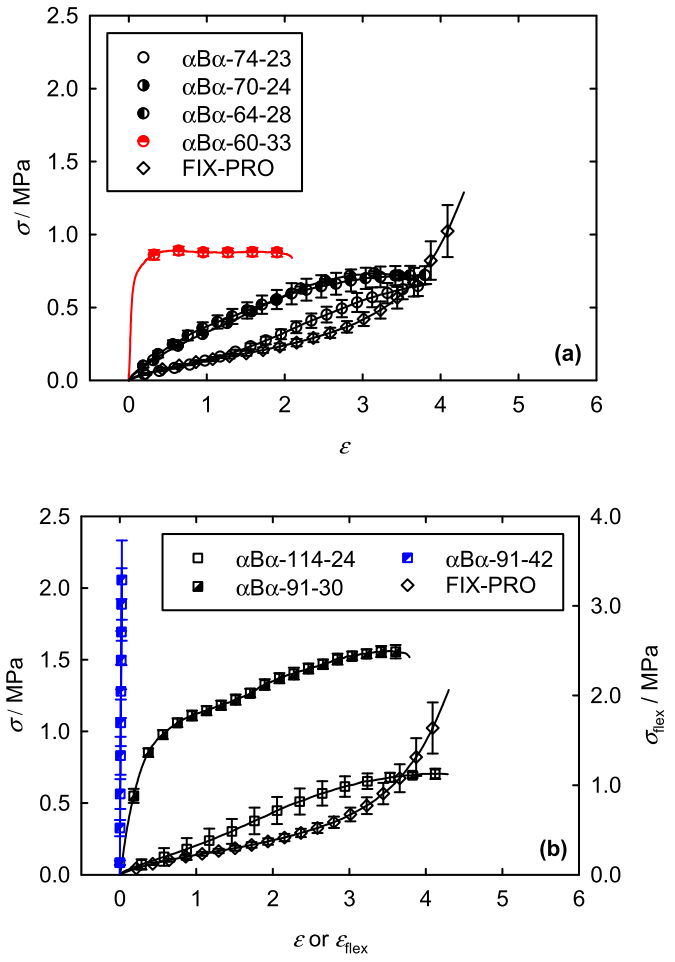


**Fig. 5.** Stress-strain curves for (a) short chain and (b) long chain αPMA triblock copolymers with varying [αPMA], showing substantial influence on mechanical performance. Results shown in black were measured using the SER, in red were measured using miniature tensile testing, and in blue using flexural testing ($\sigma_{flex}$ and $\varepsilon_{flex}$). Error bars represent ± two standard errors. (For interpretation of the references to colour in this figure legend, the reader is referred to the Web version of this article.)

tensile and possibly some shear deformations when peeled from a backing tape, and again in service to prevent detachment, and finally at the end of life when it is removed from the substrate. Throughout each of these procedures it is important that the material retains sufficient structural integrity to prevent failure. The ability to tune the mechanical properties of an elastomer by changing phase concentrations, enables optimisation of this novel material for use in a given application. Hence, gaining an understanding of the relationship between [αPMA] and tensile performance provides useful information required for the customisation of viable PSA materials.

Fig. 11 shows the changes in ultimate tensile properties and stiffness as a function of hard phase concentration [aPMA]. $E_{10\%}$ increases exponentially as a function of [αPMA], with $E_{1\%}$ for αBα-91-42 included for comparison due to failure occurring prior to 10% strain for this sample. A similar trend was also observed for $E_{1\%}$ (not shown), but measurements conducted at such low strains using the SER are considered less reliable due to challenges in determining with precision the point of zero strain. These findings are in agreement with trends exhibited by other triblock copolymer materials in the literature, including those derived from L-lactide [22] and glucose [45].

In the short chain materials, the $\sigma_{UTS}$ remains relatively constant with hard phase concentration, only increasing marginally at the highest [αPMA]. The long chain materials instead exhibit a noticeable increase in $\sigma_{UTS}$ with [αPMA]. Conversely, $\varepsilon_{UTS}$ is observed to decrease as hard phase concentration is increased, in an approximately linear manner with the long soft chain materials exhibiting a marginally larger $\varepsilon_{UTS}$ for a given concentration. The average FIX-PRO® results are indicated by a dashed line in Fig. 11 (a), (b) and (c), and the triblocks containing less than 30 wt% [αPMA] have similar ultimate tensile strains and stiffnesses to the commercial benchmark. However, only the long chain elastomer with [$\alpha$ PMA] = 30 wt% provided a comparable ultimate tensile strength.

Comparing the mechanical performance of αBα-114-24 with αBα-74-23 and αBα-70-24 as well as αBα-91-30 with αBα-64-28 and αBα-60-33 provides some insight into the relative effect of overall copolymer chain length. $\sigma_{UTS}$ and, to a lesser degree, $\varepsilon_{UTS}$ are observed to be higher for the longer chain elastomers according to Fig. 11(b) and (c). It is likely that the increased number of entanglements per molecule provides a greater degree of resistance to disentanglement and hence, to macroscopic fracture. $E_{10\%}$ does not show a clear variation with chain length.

Strain hardening, or more correctly strain *stiffening*, behaviour is observed for all the elastomers investigated in this study, as is typical of the hyperelastic nature of such materials. In order to obtain indicative material parameters, a simple model is proposed to capture the stress-strain response observed, consisting of a Gent rubber model in parallel with a constant viscosity element [46]. The Gent model allows for implementation of Gaussian hyperelasticity with finite chain extensibility, while the flow stress models the viscosity arising from flow. This form of constitutive model has been selected as it provides one of the simplest formulations for describing the tensile behaviour of these elastomers. Whilst more complex models are available and may provide a better quality of fit to experimental results, the gradual onset of failure in the samples precludes a more accurate constitutive description of their deformation at this stage.

The model was fitted to the individual experimental data in order to obtain the model parameters: the flow stress $\sigma_y$, the strain hardening modulus $G_R$, and the limiting chain extensibility in uniaxial tension $\lambda_{max}$. In uniaxial tension at constant true strain rate, the response of the model in terms of true stress $\sigma_t$ is given by [46]

$$\sigma_t = \sigma_y + G_R\left(\lambda^2 - \lambda^{-1}\right)\left(\frac{J_m}{J_m - \lambda^2 - \frac{2}{\lambda} + 3}\right) \quad (4)$$

where $\lambda$ is the stretch, equivalent to $1 + \varepsilon$, and $J_m = \lambda_{max}{}^2 + 2/\lambda_{max} - 3$.

**Table 2**
Summary of mechanical properties for αPMA triblock copolymers, with ± representing two standard errors.

| Material | Chain length | $E_{1\%}$ (MPa) | $E_{10\%}$ (MPa) | $\sigma_{UTS}$ (kPa) | $\varepsilon_{UTS}$ | Test method | No. of specimens |
|---|---|---|---|---|---|---|---|
| αBα-74-23 | Short | 0.454 ± 0.086 | 0.283 ± 0.013 | 722.0 ± 15.0 | 5.04 ± 0.77 | SER | 8 |
| αBα-70-24 | Short | 0.944 ± 0.207 | 0.558 ± 0.030 | 737.7 ± 13.9 | 3.16 ± 0.08 | SER | 8 |
| αBα-64-28 | Short | 1.049 ± 0.358 | 0.641 ± 0.073 | 754.6 ± 39.7 | 4.24 ± 0.76 | SER | 6 |
| αBα-60-33 | Short | 10.639 ± 4.549 | 7.410 ± 0.419 | 890.0 ± 29.0 | 0.57 ± 0.06 | Mini tensile | 4 |
| αBα-114-24 | Long | 0.370 ± 0.072 | 0.216 ± 0.012 | 848.2 ± 20.9 | 5.80 ± 0.44 | SER | 6 |
| αBα-91-30 | Long | 2.579 ± 1.640 | 3.370 ± 0.567 | 1585.3 ± 51.9 | 3.53 ± 0.32 | SER | 7 |
| αBα-91-42 | Long | 132.740 ± 21.214 | – | 3903.4 ± 635.8 | 0.04 ± 0.01 | Flexural | 7 |
| FIX-PRO® | – | 0.230 ± 0.092 | 0.230 ± 0.055 | 1762.5 ± 330.2 | 4.63 ± 0.08 | SER | 7 |

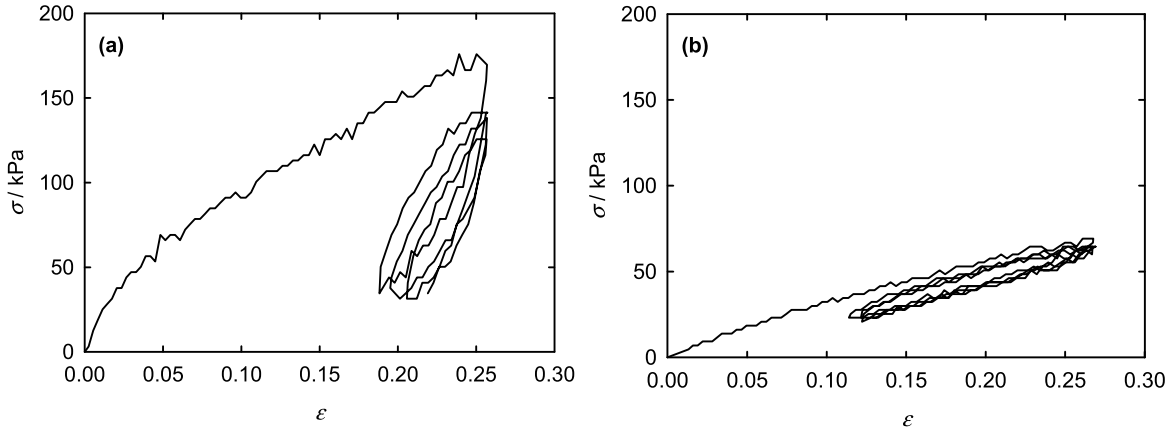


**Fig. 6.** Cyclic tensile results for (a) αBα-70-24 and (b) FIX-PRO® over four extension-relaxation cycles to 25% strain.

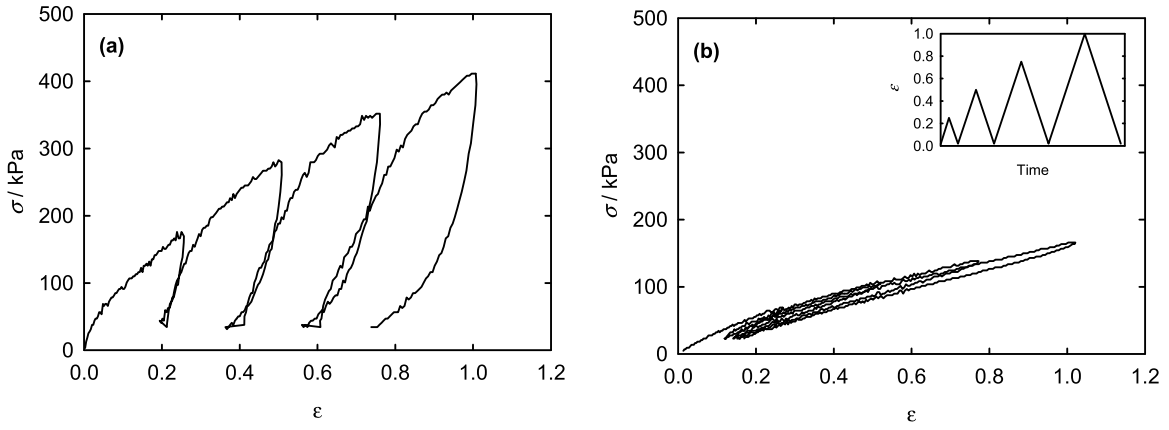


**Fig. 7.** Cyclic uniaxial tensile results for (a) αBα-70-24 and (b) FIX-PRO® over 4 cycles up to $\varepsilon = 100\%$. The inset figure in (b) shows the cyclic tensile method used to generate the results provided in both (a) and (b).

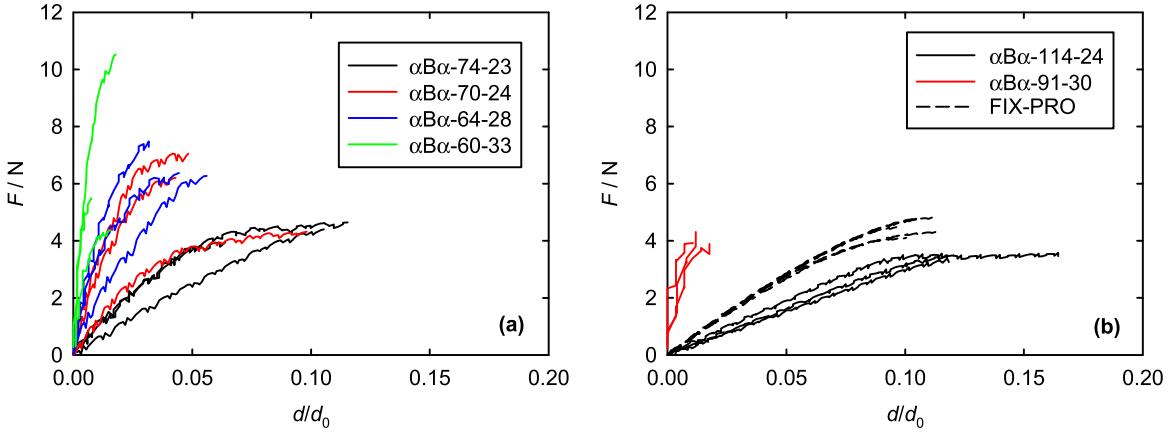


**Fig. 8.** Probe adhesion results up to $F_{max}$ for (a) short and (b) long chain elastomers with varying [αPMA]. Measurements for the commercial benchmark FIX-PRO® are included in (b).

An iterative process was utilised to reduce the range of $\lambda$ data employed in the fit until an optimal quality of fit ($R^2 > 0.999$) was achieved. Fitting data was also restricted to $\lambda > 1.1$ such that the modelled range captures only tensile performance at strains beyond the transient viscoelastic region. The model proved an excellent fit to the FIX-PRO® data as shown for representative measurements given in Fig. 12, accurately capturing the response across the full stretch range investigated. The model was also applied to triblock copolymers for which [αPMA] <

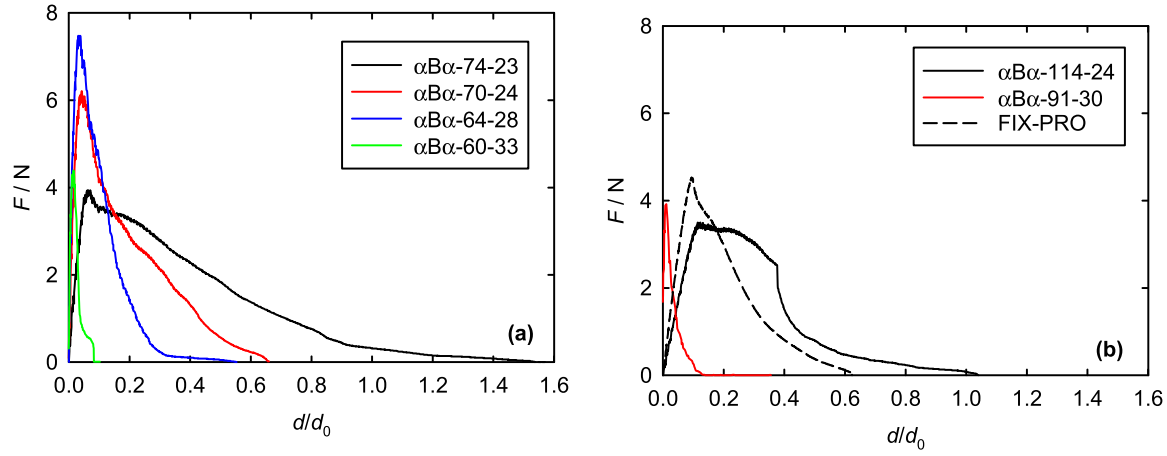


**Fig. 9.** Representative adhesion curves for (a) short and (b) long chain novel materials. Results for FIX-PRO® are also included in (b).

**Table 3**
Summary of probe adhesion results for αPMA elastomers and commercial FIX-PRO®.

| Material | Chain length | $F_{max}$ (N) | $(d/d_0)_{Fmax}$ | $W$ (kJ m$^{-3}$) |
|---|---|---|---|---|
| αBα-74-23 | Short | 4.33 ± 0.42 | 0.095 ± 0.031 | 69.3 |
| αBα-70-24 | Short | 5.86 ± 1.62 | 0.056 ± 0.044 | 52.5 |
| αBα-64-28 | Short | 6.71 ± 0.77 | 0.044 ± 0.014 | 35.2 |
| αBα-60-33 | Short | 6.80 ± 3.78 | 0.014 ± 0.006 | 5.3 |
| αBα-114-24 | Long | 3.49 ± 0.12 | 0.133 ± 0.031 | 51.1 |
| αBα-91-30 | Long | 4.04 ± 0.27 | 0.013 ± 0.004 | 5.8 |
| αBα-91-42 | Long | 0 | 0 | 0 |
| FIX-PRO® | – | 4.49 ± 0.26 | 0.11 ± 0.01 | 39.5 |

30%, showing good agreement with tensile measurements for the initial portion of the data, but deviated significantly at larger values of $\lambda$, where larger degrees of plasticity and early onset of failure occur. The fit to other triblock copolymers was poorer, and points to a difference in the nature of the cross-links, likely chemical and more permanent in nature in FIX-PRO®, and physical and less permanent in the block co-polymers. This indicates that plastic deformation of varying degrees is taking place in the block copolymers. Table 4 reports the model parameters obtained from fitting to the commercial and two novel elastomers.

Flow stresses are small for all three materials, negligible in the cases of the two novel elastomers. The strain hardening modulus is slightly smaller for the long chain material than for the short chain material, and is almost identical to that of the FIX-PRO®. Values of $G_R$ established from the Gent model are considered to be reliable, having been derived from the stress plateau at low strains ($\lambda < 3$) where the fit is of a high quality. The limiting extensibility is also observed to be lower for the long chain variant. In practice, the plasticity and gradual failure onset exhibited by the terpene-derived copolymers at large strains renders the determination of $\lambda_{max}$ challenging. There may be scope for improved modelling using a non-linear viscoelastic standard linear solid (SLS) constitutive model [47] or an Edwards-Vilgis strain energy function [48] for greater modelling versatility, once further experimental results become available.

Triblock copolymers with hard phase segments dispersed within a soft phase matrix have been found to provide the best adhesive performance due to low stiffness imparted by the soft phase enabling a more intimate contact to a hard substrate [49]. Based on this understanding, it is expected that αBα-74-23 and αBα-70-24 of the short chain materials and aBa-114-24 of the long chain materials should provide the best PSA properties. αBα-91-42 on the other hand exhibits a predominantly hard phase morphology with pockets of soft phase material encapsulated within the matrix. The continuous hard phase matrix behaves similar to a highly cross-linked structure, preventing the flow of the butyl acrylate component and resulting in poor mechanical and adhesive properties.

According to the probe adhesion findings summarised in Fig. 13(a)

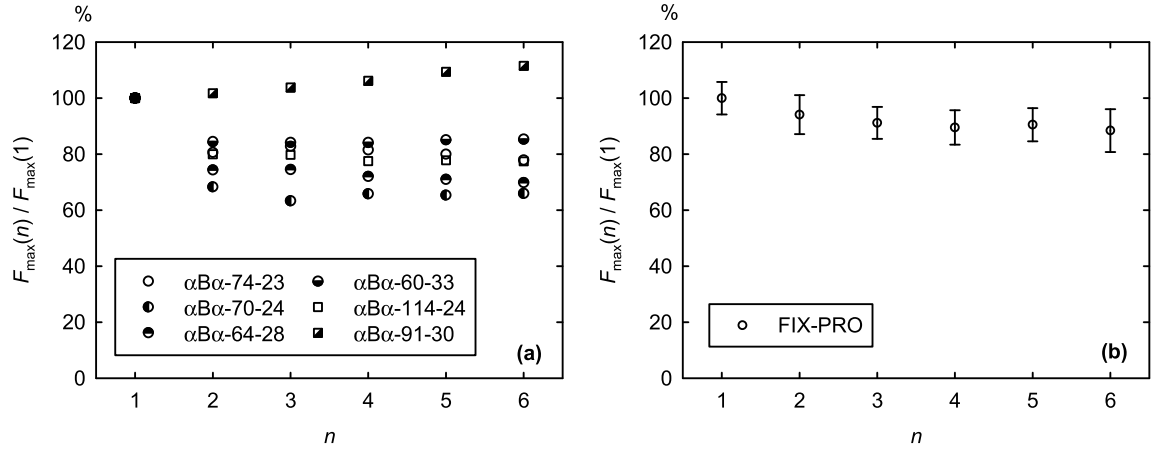


**Fig. 10.** Normalised average $F_{max}$ evolution for (a) αPMA triblock copolymers, and (b) FIX-PRO® over 6 bond-debond cycles, $n$. Error bars have been omitted from (a) for clarity and in (b) represent ± 2 standard errors.

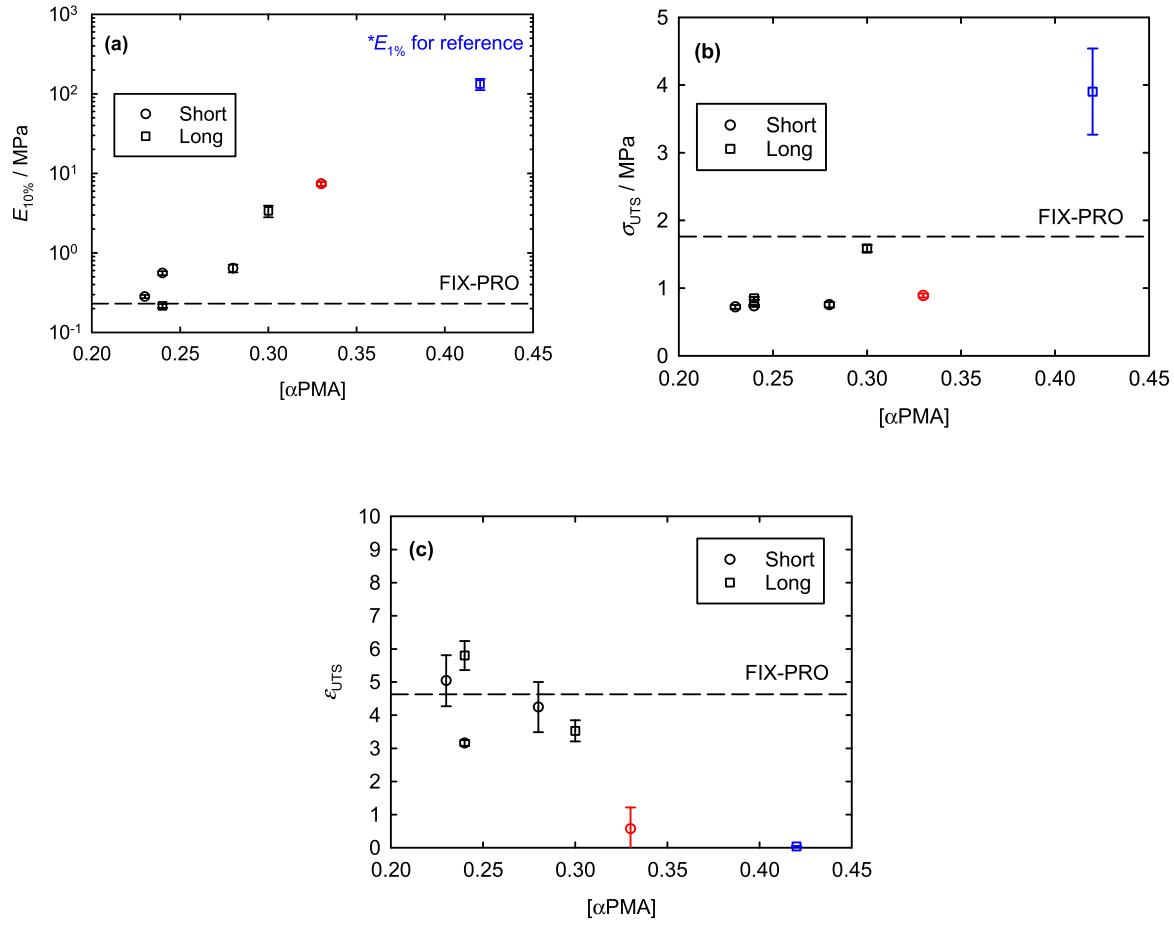


**Fig. 11.** Average values of (a) $E_{10\%}$, (b) $\sigma_{UTS}$ and (c) $\varepsilon_{UTS}$ for short (circles) and long (squares) triblock copolymers as a function of [αPMA]. Black, red and blue colouring represent SER, mini tensile and flexural experimentation respectively. Error bars represent ± two standard errors. (For interpretation of the references to colour in this figure legend, the reader is referred to the Web version of this article.)

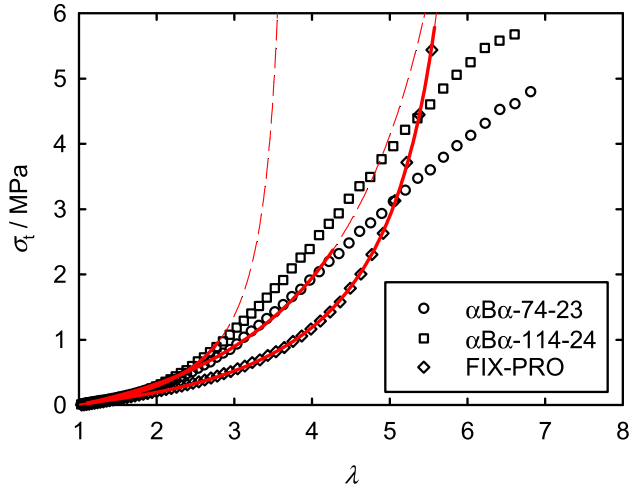


**Fig. 12.** Fig. 12: Representative tensile measurements with fitted Gent models for selected elastomers. Thin dashed red lines through points represent fitted models, with thick red lines indicating region where $R^2 > 0.997$ and from which the parameters given in Table 4 were obtained. (For interpretation of the references to colour in this figure legend, the reader is referred to the Web version of this article.)

**Table 4**
Gent model parameters generated by least-squares fitting to experimental data, where ± denotes one standard error.

| Material | Chain length | $G_R$ (kPa) | $\sigma_y$ (kPa) | $\lambda_{max}$ |
|---|---|---|---|---|
| αBα-74-23 | Short | 82.36 ± 1.28 | 0.00 ± 0.00 | 6.15 ± 0.78 |
| αBα-114-24 | Long | 70.03 ± 2.13 | 0.00 ± 0.00 | 4.02 ± 0.11 |
| FIX-PRO® | – | 69.42 ± 4.01 | 5.03 ± 3.24 | 6.25 ± 0.06 |

and (b) as a function of [αPMA], increasing [αPMA] produces a small increase in $F_{max}$ at concentrations below ~30 wt%, reaching a plateau and eventually a decrease in $F_{max}$. A continuous reduction in the normalised displacement at peak force $(d/d_0)_{Fmax}$ is also observed with increasing [αPMA]. These trends can be observed regardless of overall chain molecular weight, however $F_{max}$ values were found to be lower for the longer chain materials. One possible explanation is that increasing the molecular weight of the soft phase segment leads to an increase in the viscosity, and thus to a longer relaxation time, although this could not be confirmed by the modelling exercise. An increase in viscosity would render the polymer less able to flow and to conform to a hard surface under equivalent experimental conditions, resulting in a smaller effective contact area, and a weaker adhesive bond. It is also interesting to note that the repeatability of results for the longer chain copolymers was significantly better than for the shorter chain systems. The results shown in Fig. 13(c) indicate that increasing [αPMA] leads to a reduction in $W$ regardless of chain length, with elastomers containing <25 wt%

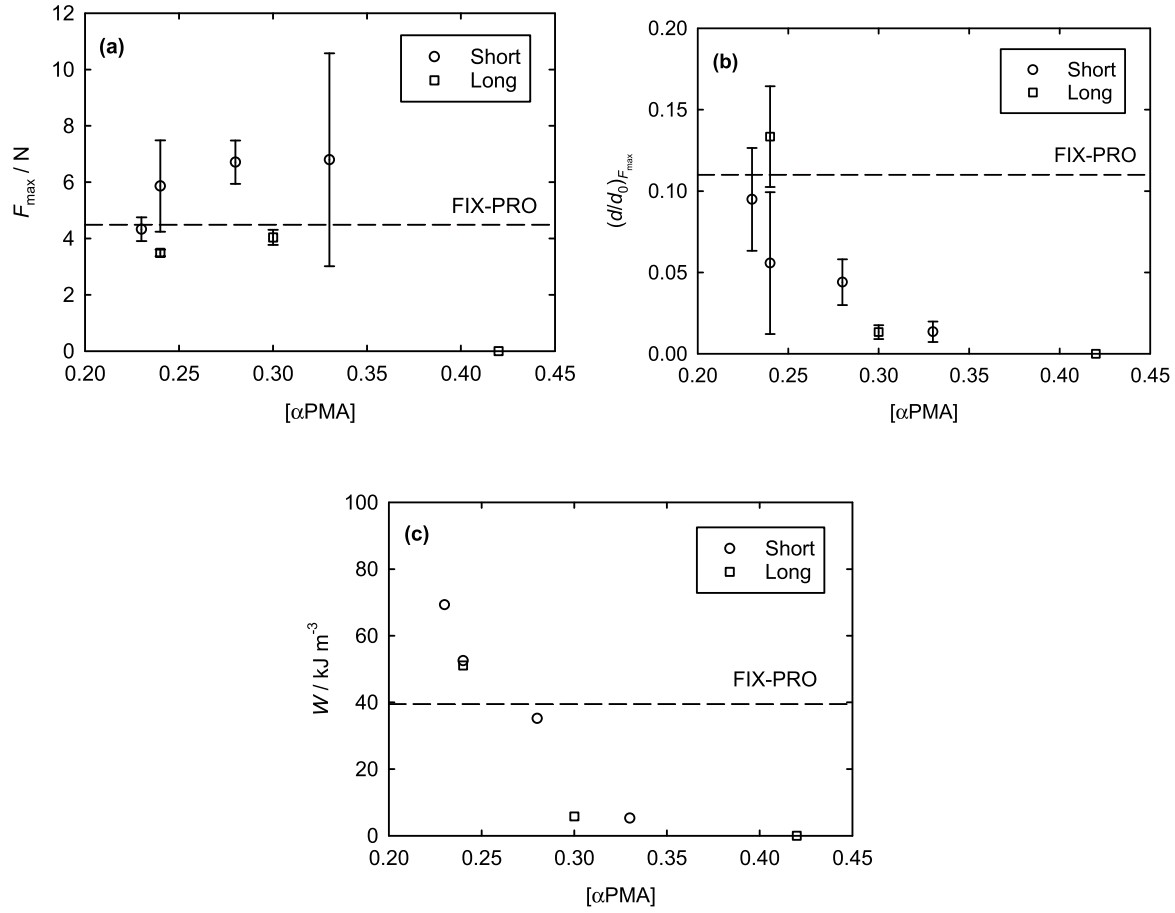


**Fig. 13.** Effect of [αPMA] and chain length on (a) peak force and (b) normalised displacement at peak force and (c) work done to separate the surfaces. Error bars represent ± two standard errors and dashed lines represent results for FIX-PRO®.

hard phase material requiring the greatest energy to cause bond failure, higher even than the FIX-PRO®.

In the same manner as for mechanical property evaluation, comparing αBα-114-24 with αBα-74-23 and αBα-70-24 as well as αBα-91-30 with αBα-64-28 and αBα-60-33 gives an indication of the effect of the overall chain length on the adhesive parameters. It is evident from Fig. 13(a) and (c) that the short chain copolymers provide a superior adhesive bond strength and slightly higher dissipated energy than for the long chain counterparts of comparable [αPMA]. The shorter chains promote faster access to a range of surface asperity sites than the longer chains, increasing bond contact area and degree of mechanical interlocking in a given time. The influence of [αPMA] on $(d/d_0)_{F\text{max}}$ is less visible from the data collected, and shows relatively similar normalised bond displacements for both long and short chains.

## 6. Conclusions

A series of long and short chain triblock copolymers of varying hard phase concentration synthesised from renewable α-pinene methacrylate and *n*-butyl acrylate have been subjected to morphological, mechanical and adhesion tests. Increasing the magnitude of the αPMA volume fraction has been shown to result in an increase in tensile and shear stiffness, ultimate tensile strength and adhesive strength. Conversely, ultimate tensile strain, normalised displacement at peak adhesive force and work done per unit volume were observed to reduce with increasing [αPMA]. Copolymer chain length was found to influence the morphology, as well as the mechanical and adhesive properties, with longer chain networks exhibiting superior ultimate tensile properties, yet lower adhesive strengths, stiffnesses and normalised displacements at peak adhesive force for a similar [αPMA]. Copolymers with a hard block fraction of 20–25 wt% have been found to perform similarly to a commercial benchmark PSA in terms of both adhesion and tensile properties, indicating possibly application suitability for these novel sustainable elastomers. Promising damping properties have also been observed in one of the investigated copolymers offering further avenues of potential application. The results suggest that the performance of these sustainable materials that can be produced from renewable feedstocks can be tuned to produce viable PSAs with a range of useful properties.

## Declaration of competing interest

The authors declare that they have no known competing financial interests or personal relationships that could have appeared to influence the work reported in this paper.

## Acknowledgements

This work was supported by the UK Engineering and Physical Sciences Research Council (EPSRC) grant EP/N019784/1.

## Appendix A. Supplementary data

Supplementary data to this article can be found online at https://doi.org/10.1016/j.polymertesting.2022.107530.

## References


[1] A.K. Singh, D.S. Mehra, U.K. Niyogi, S. Sabharwal, R.K. Khandal, Polyurethane based pressure sensitive adhesives (PSAs) using electron beam irradiation for medical application, J. Polym. Mater. 28 (4) (2011) 525–542.

[2] Z. Zhao, P. Liu, C. Zhang, X. Zhu, W. Liu, S. Li, Hot-melt pressure-sensitive adhesives based on SIS-g-PB copolymer for transdermal delivery of hydrophilic drugs, Int. J. Adhesion Adhes. 91 (2019) 72–76.

[3] C.J. Kuo, J. Chen, P. Lin, H.-T. Yen, Hot-melt pressure-sensitive adhesive for seamless bonding of nylon fabric part I : effect of a functional monomer, Textil. Res. J. 89 (6) (2019) 926–935.

[4] M. Troughton, Adhesive bonding, in: Handbook of Plastics Joining, William Andrew Publishing, 2009, pp. 145–173.

[5] Z. Czech, R. Milker, Development trends in pressure-sensitive adhesive systems, Mater. Sci. - Pol. 23 (4) (2005) 1015–1022.

[6] C. Creton, Pressure-sensitive adhesives: an introductory course, MRS Bull. 28 (6) (2003) 434–439.

[7] M.M. Feldstein, R.A. Siegel, Molecular and nanoscale factors governing pressure-sensitive adhesion strength of viscoelastic polymers, J. Polym. Sci., Part B: Polym. Phys. 50 (2012) 739–772.

[8] I. Benedek, M.M. Feldstein, Fundamentals of Pressure Sensitivity, 2009.

[9] C. Fang, K. Zhu, X. Zhu, Z. Lin, Preparation and characterization of self-crosslinking fluorinated polyacrylate latexes and their pressure sensitive adhesive applications, Int. J. Adhesion Adhes. 95 (2019) 102417.

[10] M.A. Hillmyer, W.B. Tolman, Aliphatic polyester block polymers: renewable, degradable, and sustainable, Acc. Chem. Res. 47 (2014) 2390–2396.

[11] J.M. Bolton, M.A. Hillmyer, T.R. Hoye, Sustainable thermoplastic elastomers from terpene-derived monomers, ACS Macro Lett. 3 (8) (2014) 717–720.

[12] J. Shin, M.T. Martello, M. Shrestha, J.E. Wissinger, W.B. Tolman, M.A. Hillmyer, Pressure-sensitive adhesives from renewable triblock copolymers, Macromolecules 44 (2011) 87–94.

[13] I. Webster, Recent developments in pressure-sensitive adhesives for medical applications, Int. J. Adhesion Adhes. 17 (1) (1997) 69–73.

[14] T.L. Sporleder, P.D. Goldsmitth, J. Cordier, P. Godin, Int. Food Agribus. Manag. Rev. 14 (2011) 35–50.

[15] M. Peplow, Plastic fantastic, Nature 536 (2016) 266–268.

[16] M.R. Thomsett, T.E. Storr, O.R. Monaghan, R.A. Stockman, S.M. Howdle, Progress in the synthesis of sustainable polymers from terpenes and terpenoids, Green Mater. 4 (3) (2016) 115–134.

[17] S. Kawahara, S. Akiyama, Y. Kano, Miscibility and pressure-sensitive adhesive properties of poly(vinylethylene-co-1,4-butadiene)/terpene resin blends, Polymer 32 (9) (1991) 1681–1687.

[18] M.F. Sainz, et al., A facile and green route to terpene derived acrylate and methacrylate monomers and simple free radical polymerisation to yield new renewable polymers and coatings, Polym. Chem. 7 (16) (2016) 2882–2887.

[19] J. Lu, H.U.I. Liang, W.E.I. Zhang, Q. Cheng, Synthesis of poly (b-pinene)-g-Poly (meth)acrylate by the combination of living cationic polymerization and atom transfer radical polymerization, J. Polym. Sci. Part A Polym. Chem. 41 (2003) 1237–1242.

[20] DEFRA, waste Wood, A Short Review of Recent Research, 2012.

[21] S. Wang, L. Shuai, B. Saha, D.G. Vlachos, T.H. Epps, From tree to tape: direct synthesis of pressure sensitive adhesives from depolymerized raw lignocellulosic biomass, ACS Cent. Sci. 4 (2018) 701–708.

[22] S. Lee, K. Lee, Y. Kim, J. Shin, Preparation and characterization of a renewable pressure-sensitive adhesive system derived from ε - decalactone, L-lactide, epoxidized soybean oil and rosin ester, ACS Sustain. Chem. Eng. 3 (2015) 2309–2320.

[23] E.R. Ruckel, H.G. Arlt Jr., R.T. Wojcik, The Chemistry of Tackifying Terpene Resins, Adhesion Science and Technology, 1975, pp. 395–412.

[24] M.A. Droesbeke, A. Simula, J.M. Asua, F.E. Du Prez, Biosourced terpenoids for the development of sustainable acrylic pressure-sensitive adhesives via emulsion polymerisation, Green Chem. 22 (2020) 4561–4569.

[25] J.T. Lai, D. Filla, R. Shea, Functional polymers from novel carboxyl-terminated trithiocarbonates as highly efficient RAFT agents, Macromolecules 35 (2002) 6754–6756.

[26] R.L. Atkinson, et al., RAFT polymerisation of renewable terpene (meth)acrylates and the convergent synthesis of methacrylate-acrylate-methacrylate triblock copolymers, Polym. Chem. (2021).

[27] B.V. Velcro Industries, FIX-PRO® MOUNTING TAPE, 2021 [Online]. Available: https://shop.velcro.co.uk/collections/fix-pro-mounting-tape [Accessed: 10/03/2021].

[28] J.M.G. Cowie, Block and graft copolymers, in: Comprehensive Polymer Science and Supplements, 1996, pp. 33–42.

[29] S. Mori, H.G. Barth, Size Exclusion Chromatography, first ed., Springer Berlin Heidelberg, New York, 1999.

[30] S. Noppalit, A. Simula, L. Billon, J. Asua, On the nitroxide mediated polymerization of methacrylates derived from bio-sourced terpenes in miniemulsion, a step towards sustainable products, Polym. Chem. 11 (2020) 1151–1160.

[31] N.N. Lebedev, I.S. Ufliand, Axisymmetric contact problem for an elastic layer, J. Appl. Math. Mech. 22 (3) (1958) 320–326.

[32] G.N. Greaves, A.L. Greer, R.S. Lakes, T. Rouxel, Poisson's ratio and modern materials, Nat. Mater. 10 (2011) 823–837.

[33] M.L. Sentmanat, Miniature universal testing platform : from extensional melt rheology to solid-state deformation behavior, Rheol. Acta 43 (2004) 657–669.

[34] A. Foerster, et al., UV-curable silicone materials with tuneable mechanical properties for 3D printing, Mater. Des. 205 (2021) 109681.

[35] G.Y.H. Choong, A. Canciani, D.S.A. De Focatiis, An adaptable flexural test fixture for miniaturised polymer specimens, Polym. Test. 85 (2020) 106430.

[36] J. Winters, Thumb push forces exertable by free-standing subjects, Ergonomics 29 (7) (1986) 893–902.

[37] C.C. Honeker, E.L. Thomas, Impact of morphological orientation in determining mechanical properties in triblock copolymer systems, Chem. Mater. 8 (8) (1996) 1702–1714.

[38] R. Lach, R. Weidisch, K. Knoll, Morphology and mechanical properties of binary triblock copolymer blends, J. Polym. Sci., Part B: Polym. Phys. 43 (2005) 429–438.

[39] P. Toulemonde, J. Diani, P. Gilormini, N. Desgardin, R. Neviere, Effects of small particles on the mechanical behavior and on the local damage of highly filled elastomers, J. Mater. Sci. 52 (2017) 878–888.

[40] C.P. Buckley, D.S.A. De Focatiis, C. Prisacariu, Unravelling the mysteries of cyclic deformation in thermoplastic elastomers, in: Proceedings of the 7th European Conference on Constitutive Models for Rubber, 2012, pp. 3–10.

[41] H. Schmalz, A. Boker, L. Ronald, G. Krausch, V. Abetz, Synthesis and properties of ABA and ABC triblock copolymers with glassy (A), elastomeric (B), and crystalline (C) blocks, Macromolecules 34 (25) (2001) 8720–8729.

[42] P. Karnal, P. Roberts, S. Gryska, C. King, C. Barrios, J. Frechette, Importance of substrate functionality on the adhesion and debonding of a pressure-sensitive adhesive under water, Appl. Mater. Interfaces 9 (2017) 42344–42353.

[43] A. Chiche, P. Pareige, C. Creton, Role of surface roughness in controlling the adhesion of a soft adhesive on a hard surface, Comptes Rendus l Académie des Sci. - Ser. IV - Phys. 1 (9) (2000) 1197–1204.

[44] J.H. Lai, C. Knudson, L. Hallgren, R.B. Douglas, Effect of humidity and temperature on the adhesive strength of pressure sensitive adhesives, Polym. Eng. Sci. 25 (12) (1985) 778–781.

[45] M. Nasiri, T.M. Reineke, Sustainable glucose-based block copolymers exhibit elastomeric and adhesive behavior, Polym. Chem. 7 (33) (2016) 5191–5334.

[46] A.N. Gent, A new constitutive relation for rubber, Rubber Chem. Technol. 69 (1) (1996) 59–61.

[47] C. Zener, Elasticity and Anelasticity of Metals, The University of Chicago Press, Chicago, 1948.

[48] S.F. Edwards, T. Vilgis, The effect of entanglements in rubber elasticity, Polymer 27 (4) (1986) 483–492.

[49] B.E. Gdalin, E.V. Bermesheva, G.A. Shandryuk, M. Mikhail, G.A. Shandryuk, M. M. Feldstein, Effect of temperature on probe tack adhesion: extension of the dahlquist criterion of tack, J. Adhes. 87 (2) (2011) 111–138.